Progress In Electromagnetics Research C, Vol. 107, 1–15, 2021

A Novel Synthesis Method of Sparse Nonuniform-Amplitude Concentric Ring Arrays for Microwave Power Transmission

Jianxiong Li*, Junwen Pan, and Xianguo Li

Abstract—A novel two-step synthesis method of sparse nonuniform-amplitude concentric ring arrays (SNACRAs) to maximize the beam collection efficiency (*BCE*) for microwave power transmission (MPT) is proposed in this paper. In the first step, beetle antennae search (BAS) algorithm is used to optimize the radius of each ring of the SNACRA, to obtain the maximum *BCE* and the equivalent continuous excitation of each ring. In the second step, we find the least array element on each ring to discretize the continuous excitation on each ring by using the binary search (BS) algorithm directly under the restriction conditions and then find the excitation of each element. Through the above two steps of optimization, the optimal synthesized parameters of the SNACRA, including the maximum *BCE*, layout, excitation, and power pattern, can be obtained highly efficiently. Many representative numerical results under different ring numbers, apertures, and receiving areas are presented. Comparing these numerical results with those of other three arrays for MPT, it is proved that the SNACRA synthesized by the two-step method can get higher *BCE* with less elements and have a relatively simple feed network.

1. INTRODUCTION

Microwave power transmission (MPT), as a promising technology of long-distance wireless power transmission, delivers a large amount of electromagnetic power at microwave frequencies from one place to another [1–3]. It can be used to charge for some mobile devices, such as mobile phones, laptops, electric vehicles, and unmanned aerial vehicles [4–6]. In addition, MPT is a key technology to establish solar power satellites (SPS) [7]. Due to its wide application scenarios, more and more scholars pay more attention to MPT [8–10]. Different from communication systems, MPT systems focus on energy transfer rather than information transmission. Therefore, high-efficiency power transmission is significant to develop an MPT system. Although the total efficiency of MPT systems is related to many parameters [11], beam collection efficiency (*BCE*), which is defined as the ratio of the power captured by receiving antenna to the power radiated by transmitting antenna, is a vital parameter for MPT systems.

For most MPT systems, array antennas are usually adopted for higher *BCE* instead of a single antenna. By solving the generalized eigenvalue problem, the maximum *BCE* and the corresponding optimal excitation of the planar array can be obtained [12]. However, since the excitation of each element in the asymmetrical position is different, there is no choice but to design an amplifier and a phase shifter for each element feed circuit separately [13]. Undoubtedly, this will increase the complexity of the feed network of the transmitting array. In order to simplify the feed network, a random-located uniform-excitation rectangular array (RURA) is adopted for MPT in [14]. The RURA can achieve *BCE* of 89.96% after optimizing element positions, which is about 5.39% lower than that of the nonuniform-excitation array in [12] under the same aperture and receiving area. Nevertheless, the calculation amount

Received 18 September 2020, Accepted 29 October 2020, Scheduled 11 November 2020
* Corresponding author: Jianxiong Li (lijianxiong@tiangong.edu.cn).
The authors are with the Tianjin Key Laboratory of Optoeletronic Detection Technology and Systems, School of Electronics and Information Engineering, Tiangong University, China.

for synthesizing the RURA could increase with its element number rapidly. Moreover, regular fully-populated transmitting arrays in [12, 14] need a large number of array elements, which could increase the cost of MPT systems. In order to reduce the number of elements and the amount of computation, Zhou et al. discussed the synthesis of a sparse uniform amplitude concentric ring array (SUACRA) for MPT in [15]. Due to structural circle-symmetry characteristic, the computational complexity of the SUACRA synthesis can be cut down. Moreover, the SUACRA adopts the sparse layout, which can greatly reduce the number of elements. Yet, the maximum *BCE* obtained from the SUACRA is much lower than that in [12]. As a result, although the array with uniform excitation proposed in [14, 15] has a simple feed network, there is a marked decline in terms of *BCE*. This is undesirable in the MPT system, because it pays much attention to efficiency.

In this paper, a sparse nonuniform-amplitude concentric ring array (SNACRA) is proposed. Compared to the uniform-amplitude concentric ring array in [15], the nonuniform-amplitude concentric ring array has different weights for elements on different rings, but has equal weights for elements on the same ring. Not only does this nonuniform feeding structure for concentric ring array acquire higher *BCE*, but also its feed network only needs to add a control point for each ring, which hardly increases the complexity of the feed network. Besides, as mentioned in [16], not every element in the transmitting array contributes to the *BCE*. In order to further reduce the element number of transmitting array, t sparse layout is adopted for the SNACRA, which can greatly reduce the number of elements without sacrificing *BCE*. For synthesizing the proposed SNACRA, we discuss a fast and efficient synthesis method in this paper. This novel method consists of two steps, which are based on the beetle antennae search (BAS) algorithm [17] and binary search (BS) algorithm. The SNACRA synthesized by the proposed method can get higher *BCE* with fewer elements and have a relatively simple feed network.

2. MATHEMATICAL DERIVATION OF THE MAXIMUM *BCE* OF THE SNACRA

The model of the MPT system is depicted in Figure 1. Within this model, the SNACRA transmitting antenna is located in the XOY plane, and the receiving antenna is in the far field of the transmitting array. The SNACRA is composed of rings with different radii, and the radius of the largest ring is equal to L. The elements on the same ring distribute with uniform spacing. Then, the array factor of the SNACRA can be expressed as

$$F(\theta,\varphi)=\sum_{m=1}^{M}\sum_{n=1}^{N_m} I_m e^{jk\rho_m \sin(\theta)\cos(\varphi-\varphi_{mn})} \tag{1}$$

where N_m, I_m, and ρ_m are, respectively, the element number, excitation, and the radius of the mth ring; $\varphi_{mn}=2\pi n/N_m$ denotes the azimuth angle of the nth element located on $k=2\pi/\lambda$ (λ is the

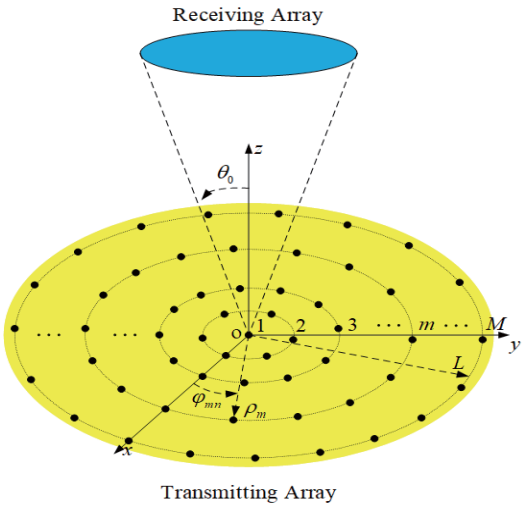

Figure 1. Geometry of the MPT system.

wavenumber); and θ and φ represent the radiation elevation angle and azimuth angle, respectively. It is worth noting that in SUACRA [15], the value of I_m of each element is the same, but in SNACRA I_m is equal on the same ring and unequal on different rings. $\rho_1 = 0$ means that there is an element at the center of the SNACRA. BCE is defined as the ratio of the power radiated on a fixed angle to the total radiated power, which can be written as

$$BCE \triangleq \frac{P_\Psi}{P_\Omega} = \frac{\int_\Psi P(\theta,\varphi)d\psi}{\int_\Omega P(\theta,\varphi)d\Omega} = \frac{\int_\Psi |F(\theta,\varphi)|^2 d\Psi}{\int_\Omega |F(\theta,\varphi)|^2 d\Omega} \tag{2}$$

where P_Ψ and P_Ω are, respectively, the power captured from the receiving area $\Psi \triangleq \{(\theta,\varphi) : 0 \le \theta \le \theta_0, 0 \le \varphi \le 2\pi\}$ and the power radiated throughout the whole visible range $\Omega \triangleq \{(\theta,\varphi) : 0 \le \theta \le \pi, 0 \le \varphi \le 2\pi\}$.

The array factor of the SNACRA can be expressed by the Bessel series [18], which can be rewritten as

$$F(\theta,\varphi) = \sum_{m=1}^{M} I_m N_m \sum_{n=-\infty}^{\infty} J_{nN_m}(k\rho_m \sin(\theta)) e^{jnN_m(\frac{\pi}{2}-\varphi)} \tag{3}$$

where $J_{nN_m}(\cdot)$ is the nN_m order Bessel function. According to the property of Bessel function, if the number of elements on the mth ring, N_m, is large enough, Eq. (3) can be approximately simplified as [18]

$$F(\theta,\varphi) \approx F_{J_0}(\theta) = \sum_{m=1}^{M} \omega_m J_0(k\rho_m \sin(\theta)) \tag{4}$$

where $J_0(\cdot)$ corresponds to the zero-order Bessel function; $F_{J_0}(\theta)$ is the approximate array factor with zero order Bessel function; and ω_m denotes the equivalent weight of the mth ring, which can be written as

$$\omega_m = I_m N_m \tag{5}$$

It is noteworthy that the value of $F_{J_0}(\theta)$ is not related to φ. The power approximate error ξ between $F(\theta,\varphi)$ and $F_{J_0}(\theta)$ can be defined as

$$\xi \triangleq \frac{\left| \int_0^{2\pi} \int_0^{\pi} |F(\theta,\varphi)|^2 d\theta d\varphi - 2\pi \int_0^{\pi} |F_{J_0}(\theta)|^2 d\theta \right|}{\int_0^{2\pi} \int_0^{\pi} |F(\theta,\varphi)|^2 d\theta d\varphi} \tag{6}$$

If we write $F_{J_0}(\theta)$ in the form of matrix, Eq. (4) can be rewritten as

$$F_{J_0}(\theta) = \mathbf{W}\mathbf{J}^H(\theta) \tag{7}$$

where $\mathbf{W} = [\omega_1, \omega_2, \cdots, \omega_M]$ is the equivalent weight vector, $\mathbf{J}(\theta) = [J_0(k\rho_1 \sin(\theta)), J_0(k\rho_2 \sin(\theta)), \ldots, J_0(k\rho_M \sin(\theta))]$ is the array steering vector; and $(\cdot)^H$ denotes the conjugate transposition of the matrix. Substituting Eq. (7) into Eq. (2), we have

$$BCE \approx \frac{\int_\Psi |F_{J_0}(\theta)|^2 d\Psi}{\int_\Omega |F_{J_0}(\theta)|^2 d\Omega} = \frac{\int_\Psi \mathbf{W}\mathbf{J}^H(\theta)\mathbf{J}(\theta)\mathbf{W}^H d\Psi}{\int_\Omega \mathbf{W}\mathbf{J}^H(\theta)\mathbf{J}(\theta)\mathbf{W}^H d\Omega} = \frac{\mathbf{W}\mathbf{A}\mathbf{W}^H}{\mathbf{W}\mathbf{B}\mathbf{W}^H} \tag{8}$$

where

$$\begin{cases} \mathbf{A} \triangleq \int_\Psi \mathbf{J}^H(\theta)\mathbf{J}(\theta)d\Psi \\ \mathbf{B} \triangleq \int_\Omega \mathbf{J}^H(\theta)\mathbf{J}(\theta)d\Omega. \end{cases} \tag{9}$$

$\mathbf{A}$ and $\mathbf{B}$ are both $M \times M$ matrixes. Their values are related to θ_0 and the radius vector $\mathbf{R} = [\rho_1, \rho_2, \ldots, \rho_M]^H$, when the wavenumber k is fixed. Moreover, $\mathbf{A}$ and $\mathbf{B}$ satisfy: (I) $\mathbf{A}$ and $\mathbf{B}$ are Hermitian matrices, because $\mathbf{A} = \mathbf{A}^H$ and $\mathbf{B} = \mathbf{B}^H$; (II) $\mathbf{A}$ and $\mathbf{B}$ are positive-definite matrices, because $\mathbf{WAW}^H > 0$ and $\mathbf{WBW}^H > 0$ whatever $\mathbf{W} \neq 0$.

When the value of $\mathbf{R}$ is known, the position of each ring in the SNACRA is fixed. According to [12], given the value of θ_0, the maximum BCE of the SNACRA with fixed ring positions, $BCE_{\max}$, is equal to the maximum generalized eigenvalues (real) of $\mathbf{A}$ to $\mathbf{B}$, and the optimal equivalent weight vector, $\mathbf{W}_{opt}$, is the eigenvector corresponding to the maximum generalized eigenvalues, i.e.,

$$\mathbf{AW}_{opt} = \eta_{\max}\mathbf{BW}_{opt} \tag{10}$$

$$BCE_{\max} = \eta_{\max} \tag{11}$$

3. TWO-STEP METHOD FOR OPTIMAL SYNTHESIS OF THE SNACRA

As mentioned in Section 2, the values of $BCE_{\max}$ and $\mathbf{W}_{opt}$ are obtained under the condition that the position of each ring of the SNACRA and the receiving region (i.e., the values of $\mathbf{R}$ and θ_0) are known. However, if $\mathbf{R}$ and θ_0 are variables, the values of $BCE_{\max}$ and $\mathbf{W}_{opt}$ will vary with $\mathbf{R}$ and θ_0. As a result, given the size of receiving region, we can get higher BCE by optimizing the radius vector $\mathbf{R}$ of the SNACRA. In this paper, we solve the problem of the optimal synthesis of the SNACRA for maximizing BCE by the following two steps.

3.1. Step 1: Optimizing Radius of Each Ring To Maximize BCE

Taking the minimum element spacing constraint into consideration, the ring number M should satisfy the following condition

$$M \leq \left\lfloor \frac{L}{d_{\min}} \right\rfloor \tag{12}$$

where $d_{\min}$ represents the constraint value of the minimum element spacing, and $\lfloor \cdot \rfloor$ stands for the rounding number to the nearest integer less than or equal to the number. When the values of M, L, θ_0, and $d_{\min}$ are given, the problem of optimal synthesis of the SNACRA in step 1 can be concluded as an optimization problem. The corresponding optimization model can be established as follows:

$$\begin{cases} \text{find } \ \mathbf{R} = [\rho_1, \rho_2, \ldots, \rho_M]^H \\ \text{maximize } \ BCE^S_{\max} = BCE_{\max}(\mathbf{R}) \\ \text{subject } \ \text{(a) } \rho_1 < \rho_2 < \ldots < \rho_M \\ \qquad\quad \text{(b) } \rho_1 = 0, \rho_M = L \\ \qquad\quad \text{(c) } \rho_{m+1} - \rho_m \geq d_{\min}, \ m = \{1, 2, \ldots, M-1\} \end{cases} \tag{13}$$

where $\mathbf{R} = [\rho_1, \rho_2, \ldots, \rho_M]^H$ is the optimization variable, and $BCE^S_{\max}$ represents the maximum BCE of the SNACRA with random ring positions. The aim of above optimization model is to find the optimal $\mathbf{R}$ to maximize $BCE^S_{\max}$ under constrains of (a), (b), and (c) in Eq. (13). In order to ensure high BCE and maintain the same array aperture after implementing sparse arrangement, the first ring radius is set as 0, and the last equals L. The minimum spacing constraint is guaranteed by constrain of (c) in Eq. (13).

In order to simplify the optimization model, $\mathbf{R}$ can be transformed as

$$\mathbf{R} = \begin{bmatrix} \rho_1 \\ \rho_2 \\ \rho_3 \\ \vdots \\ \rho_{M-1} \\ \rho_M \end{bmatrix} = \begin{bmatrix} d_1 \\ d_2 + d_{\min} \\ d_3 + 2d_{\min} \\ \vdots \\ d_{M-1} + (M-2)d_{\min} \\ d_M + (M-1)d_{\min} \end{bmatrix} = \mathbf{D} + \mathbf{D}_{\min} \tag{14}$$

where $\mathbf{D} = [d_1, d_2, \ldots, d_M]^H$ and $\mathbf{D}_{\min} = [0, d_{\min}, 2d_{\min}, \ldots, (M-1)d_{\min}]^H$. The optimization model can be rewritten as

$$\begin{cases} \text{find } \mathbf{D} = [d_1, d_2, \ldots, d_M]^H \\ \text{maximize } BCE^S_{\max} = BCE_{\max}(\mathbf{D} + \mathbf{D}_{\min}) \\ \text{subject (a) } d_1 < d_2 < \cdots < d_M \\ \qquad\quad \text{(b) } d_1 = 0, d_M = L - (M-1)d_{\min} \\ \qquad\quad \text{(c) } 0 \le d_m \le L - (M-2)d_{\min}, \\ \qquad\qquad m = \{2, 3, \cdots, M-1\} \end{cases} \tag{15}$$

where the optimization variable changes from $\mathbf{R}$ to $\mathbf{D}$, and the search range of the radius changes from $(0, L)$ to $(0, (M-1)d_{\min})$. The minimum element spacing constraint no longer needs to be considered, which greatly simplifies the optimization process.

Due to the strongly nonlinear relationship between the array factor and ring positions [19], the optimization model in step 1 is a multi-dimensional and non-convex one. Evolutionary algorithms, such as genetic algorithm (GA) [20], is suitable for this problem. However, beetle antennae search (BAS) algorithm, a new global optimization algorithm proposed in 2017 [17], is adopted in this paper. This is the first time it has been used in arrays synthesis. Compared to GA, it is a non-group search algorithm and can implement global search only by one beetle, which can substantially improve the optimization speed. For more information about BAS algorithm, readers can refer to [17].

3.2. Step 2: Solving the Element Number and the Amplitude

After solving the optimization model in step 1 by BAS algorithm, the maximum BCE, $BCE^S_{\max}$, the optimal equivalent weight vector, $\mathbf{W}^S_{opt}$, and the radius vector $\mathbf{R}^S_{opt}$ of the SNACRA can be obtained. It is pointed out that $\mathbf{W}^S_{opt}$ is an intermediate quantity, and it can be used to solve the element number N_m and amplitude I_m on the mth ring.

As mentioned above, only when N_m is large enough and the approximate error ξ small enough, the BCE calculated by the approximate array factor $F_{J_0}(\theta)$ is close to the actual BCE. Moreover, with the increase of N_m, ξ will become smaller, and $BCE^S_{\max}$ solved in step 1 will become more accurate. Nevertheless, too many elements will inevitably lead to higher cost for MPT systems. Accordingly, it is necessary to find the tradeoff between ξ and N_m.

For the aim of step 2, we record the approximate error of the mth ring as ξ_m. According to Eq. (6), the expression of ξ_m can be written as

$$\xi_m = \frac{\displaystyle\int_0^{2\pi}\int_0^{\pi}\left|\sum_{n=1}^{N_m} I_m e^{jk\rho_m \sin(\theta)\cos(\varphi-\varphi_{mn})} - \omega_m J_0(k\rho_m \sin(\theta)\right|^2 d\theta d\varphi}{\displaystyle\int_0^{2\pi}\int_0^{\pi}\left|\sum_{n=1}^{N_m} I_m e^{jk\rho_m \sin(\theta)\cos(\varphi-\varphi_{mn})}\right|^2 d\theta d\varphi} \tag{16}$$

Substituting Eq. (5) into Eq. (16), we obtain

$$\xi_m = \frac{\displaystyle\int_0^{2\pi}\int_0^{\pi}\left|\sum_{n=1}^{N_m} e^{jk\rho_m \sin(\theta)\cos(\varphi-\varphi_{mn})} - N_m J_0(k\rho_m \sin(\theta)\right|^2 d\theta d\varphi}{\displaystyle\int_0^{2\pi}\int_0^{\pi}\left|\sum_{n=1}^{N_m} e^{jk\rho_m \sin(\theta)\cos(\varphi-\varphi_{mn})}\right|^2 d\theta d\varphi} \tag{17}$$

As can be seen from Eq. (17), the value of ξ_m is only related to ρ_m and N_m rather than I_m. Therefore, the approximate error on each ring can be calculated by substituting each radius in $\mathbf{R}^S_{opt}$ obtained in

step 1. Then, the problem in step 2 can be formulated as

$$\begin{cases} \text{find } N_m(m=2,\cdots,M) \\ \text{minimize } N_m \\ \text{subject (a) } \xi_m \le \xi_t \\ \qquad\quad \text{(b) } 1 < N_m \le N_m^{\max} N_m \in N^+ \end{cases} \tag{18}$$

where ξ_t is a threshold value of approximate error, N^+ the set of all positive integers, and $N_m^{\max} = \lfloor 2\pi\rho_m/d_{\min} \rfloor$ the maximum element number that can be placed on the mth ring under the constraint of $d_{\min}$. The optimization problem in Eq. (18) can be described as follows: finding the minimum N_m from the domain $[1, N_m^{\max}]$ until ξ_m is less than or equal to the threshold ξ_t. If ξ_m is still larger than ξ_t when $N_m = N_m^{\max}$, the element number on the mth ring can be set as $N_m^{\max}$. Because N_m is a positive integer and decreases with ξ_m, the binary search (BS) algorithm can solve this linear optimization problem directly. According to our experience, the value of ξ_t can be set to 10^{-5}.

After finding the optimal value of N_m, I_m can be solved by the intermediate quantity $\mathbf{W}_{opt}^S$ obtained in step 1 according to Eq. (5). Through the above two steps, the optimal synthesis problem of the SNACRA can be solved.

4. SIMULATION AND NUMERICAL RESULTS ANALYSIS

The objective of this section is threefold. Firstly, we use the two-step synthesis method proposed in this paper to synthesize the SNACRA under different parameters and analyze the corresponding numerical results. Secondly, in order to prove the performance of the SNACRA and the validity of the two-step synthesis method, the numerical results of the SNACRA will be compared to those of three types of circular aperture arrays under the same parameters. The first array is nonuniform-amplitude fully-populated concentric ring arrays (NFCRA). The second array is the SUACRA in [15]. The third array is the circular-aperture square-lattice nonuniform-excitation planar array (CSNPA) in [12]. Finally, to show the excellent performance of BAS algorithm for synthesizing the SNACRA, we compare BAS algorithm with GA. The CPU adopted for all simulations is Intel Core i7-4510U at 2.0 GHz with 8 GB RAM, and the numerical analysis software is MATLAB R2018a in this paper.

In order to facilitate the comparison of the results later, we introduce two evaluating indicators. One is the sparsity ratio γ, which is a key evaluating indicator for sparse arrays. It is defined as the ratio of elements used in sparse layout to that used in fully-populated layout under the same aperture. The other is CSL, which is defined as the highest side-lobe level outside the receiving area Ψ. According to [12], CSL (dB) can be written as

$$CSL(\text{dB}) = 10\lg\frac{\max_{\theta,\varphi\notin\Psi}|F(\theta,\varphi)|^2}{\max_{\theta,\varphi\in\Omega}|F(\theta,\varphi)|^2} \tag{19}$$

4.1. Effects of Different Parameters on Synthesized Results

The ring number M determines the sparsity ratio γ of the SNACRA to some extent. In order to find the optimal ring number M_{opt} of the SNACRA, we study the effect of M on synthesized results of the SNACRA in the first experiment. In this experiment, we selected an SNACRA with a aperture diameter D of 9.5λ, and the values of $d_{\min}$ and the radius of collection area r_0 ($r_0 = \sin\theta_0$) are set to half wavelength $\lambda/2$ and 0.2, respectively. Figure 2 shows the behavior of synthesized BCE and the total element number N of the SNACRA varying with M. The value of the BCE increases with M when $M \le 7$, and tends to be stable when $M > 7$. By contrast, the value of N grows with M. As a result, the optimal ring number M_{opt} is equal to 7. Moreover, repeating above experiment under different aperture diameters, we find that the value of BCE will not rise when M is greater than a positive integer, and the positive integer is M_{opt}. So, we can find M_{opt} for different aperture diameters according to the curve of BCE varying with M.

Unlike the SNACRA, M_{opt} of the NFCRA can be calculated directly by the formula $M_{opt} = \lfloor D/2d_{\min} \rfloor$. The values of M_{opt} of the SNACRA and the NFCRA under different D are shown in

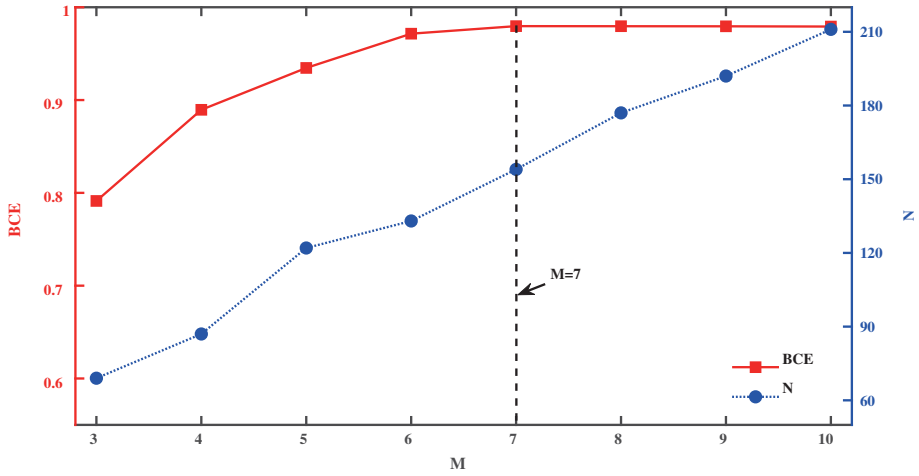

Figure 2. Behavior of BCE and N of the SNACRA ($D = 9.5\lambda$ and $r_0 = 0.2$) versus the ring number M.

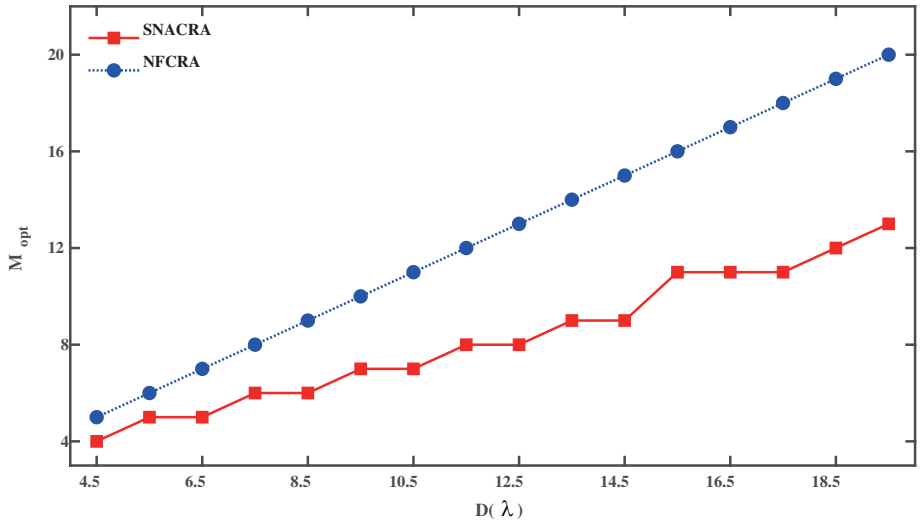

Figure 3. Variation of the optimal ring number M_{opt} of the SNACRA and the NFCRA versus the aperture diameter.

Figure 3. From Figure 3, we can see that the ring number of the SNACRA is smaller than that of the NFCRA under the same aperture.

After the ring number M is set as the corresponding optimal value, we study the effect of other parameters on the synthesized results of the SNACRA. Table 1 and Figure 4 show the synthesized results from a larger set of experiments at different aperture diameters $D \in \{4.5\lambda, 5.5\lambda, \ldots, 18.5\lambda, 19.5\lambda\}$ and receiving area radii $r_0 \in \{0.025, 0.05, 0.1, 0.2, 0.4\}$. In Table 1, BCE^1 represents the approximate value of BCE obtained by the method proposed in this paper, BCE^2 the actual BCE calculated by substituting the synthesized parameters into the definition formula (2), and $e = (BCE^1 - BCE^2)/BCE^2$ the error ratio between them, which can measure the accuracy of the proposed method. Some conclusions can be drawn from Table 1 and Figure 4: (I) The BCE obtained by the proposed method is very accurate, because BCE^1 is very close to BCE^2, and the error ratio e is less than 10^{-4} for any aperture and receiving area in Table 1; (II) For an SNACRA transmitting array given aperture size, increasing the size of the receiving area can result in higher BCE and lower CSL, and element numbers in different receiving areas have some differ-

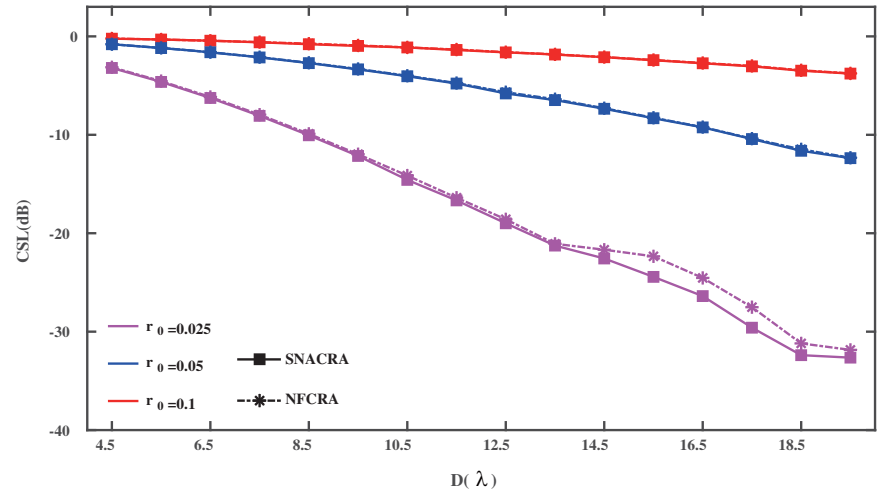

(a)

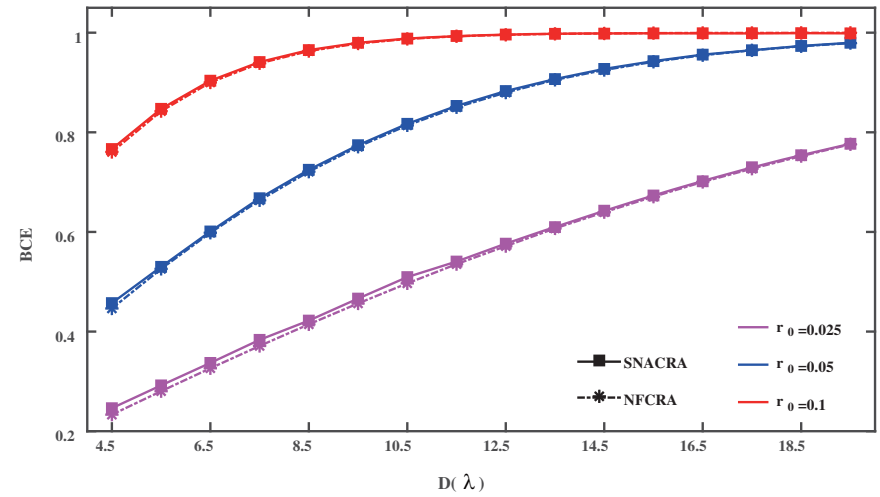

(b)

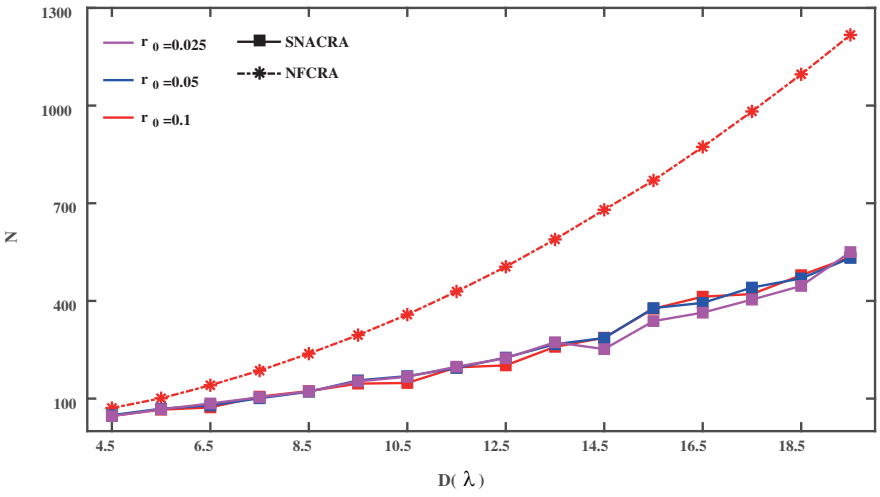

(c)

Figure 4. Synthesized numerical results of the SNACRA and the NFCRA under different aperture diameters (a) *BCE*, (b) *CSL*, (c) *N*.

Table 1. Synthesis numerical results of the SNACRA under different aperture size and receiving area.

D (λ)	r_0	M	N	BCE^1 (%)	BCE^2 (%)	CSL (dB)	e
4.5	0.1	4	46	76.6499	76.6493	−3.21	7.67×10^{-6}
	0.2		48	97.8674	97.8672	−12.08	2.14×10^{-6}
	0.4		48	99.9977	99.9969	−41.23	7.22×10^{-6}
9.5	0.05	7	156	77.4457	77.4456	−3.35	2.17×10^{-6}
	0.1		153	97.9596	97.9588	−12.15	7.64×10^{-6}
	0.2		157	99.9974	99.9926	−42.05	4.80×10^{-5}
19.5	0.025	13	534	77.7052	77.6975	−3.76	6.43×10^{-5}
	0.05		532	98.0012	97.9960	−12.38	5.31×10^{-5}
	0.1		550	99.845	99.8173	−32.64	2.83×10^{-5}

ence (e.g., $[BCE, N, CSL]\,|_{r_0=0.1,D=4.5\lambda} = [76.65\%, 46, -3.21\,\text{dB}]$ vs. $[BCE, N, CSL]\,|_{r_0=0.2,D=4.5\lambda} = [97.96\%, 48, -12.08\,\text{dB}]$ vs. $[BCE, N, CSL]\,|_{r_0=0.4,D=4.5\lambda} = [99.99\%, 48, -41.23\,\text{dB}]$, and their synthesized layout, excitation and power pattern are shown in Figure 5, Figure 6, and Figure 7.); (III) When the receiving area Ψ is given, BCE and element number N of the SNACRA increase with circular aperture diameter D, while CSL decreases with D (e.g., $[BCE, N, CSL]\,|_{D=4.5\lambda,r_0=0.1} = [76.65\%, 46, -3.21\,\text{dB}]$ vs. $[BCE, N, CSL]\,|_{D=9.5\lambda,r_0=0.1} = [97.96\%, 153, -12.15\,\text{dB}]$ vs. $[BCE, N, CSL]\,|_{D=19.5\lambda,r_0=0.1} = [99.85\%, 550, -32.64\,\text{dB}]$, and their synthesized layout, excitation and power pattern are given in Figure 5, Figure 8, and Figure 9).

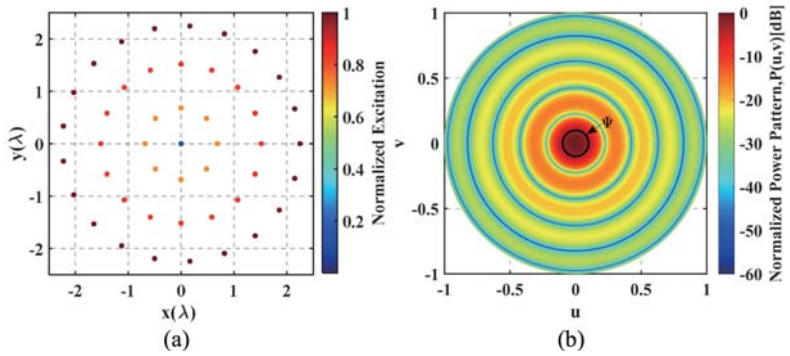

Figure 5. Synthesized results of the SNACRA ($D = 4.5\lambda$ and $r_0 = 0.1$) (a) layout and weight, (b) radiation power.

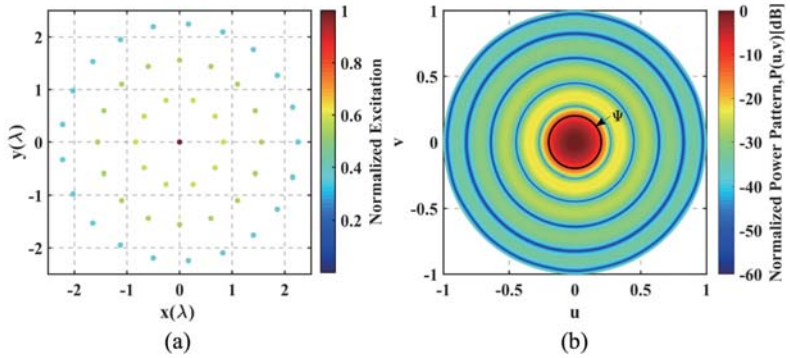

Figure 6. Synthesized results of the SNACRA ($D = 4.5\lambda$ and $r_0 = 0.2$) (a) layout and weight, (b) radiation power.

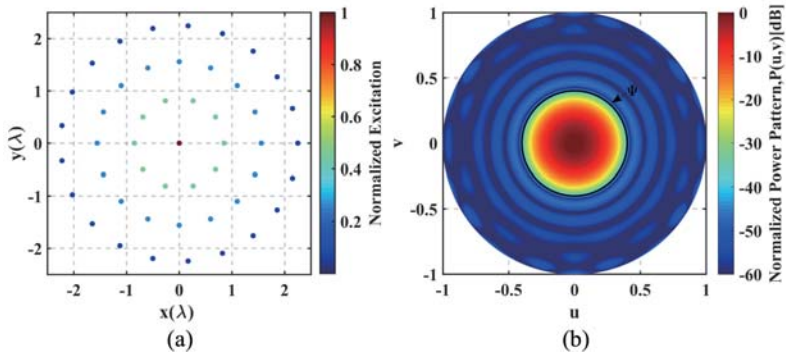

Figure 7. Synthesized results of the SNACRA ($D = 4.5\lambda$ and $r_0 = 0.4$) (a) layout and weight, (b) radiation power

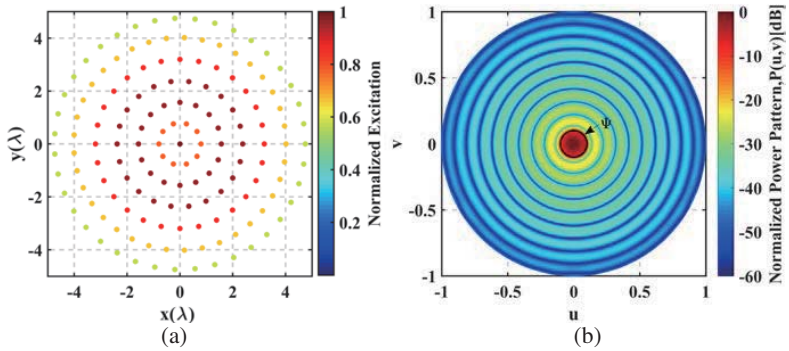

Figure 8. Synthesized results of the SNACRA ($D = 9.5\lambda$ and $r_0 = 0.1$) (a) layout and weight, (b) radiation power.

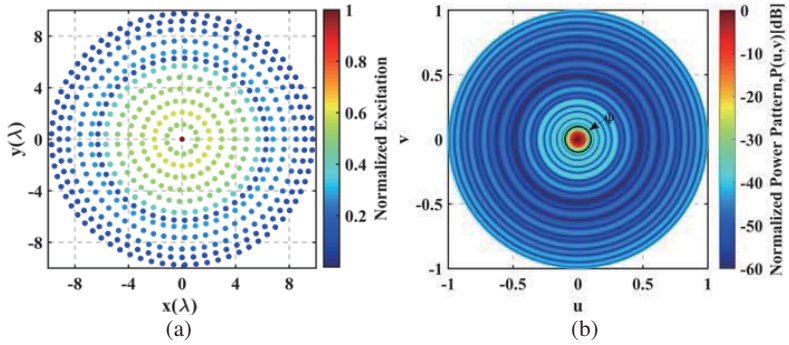

Figure 9. Synthesized results of the SNACRA ($D = 19.5\lambda$ and $r_0 = 0.1$) (a) layout and weight, (b) radiation power.

4.2. Comparison with Three Circular Aperture Arrays

In order to prove that the SNACRA is a cost-efficient option for MPT systems, we compare its synthesized results with those of the NFCRA in Table 2 and Figure 4. Obviously, (I) the SNACRA can achieve the same or slightly better performance with fewer elements than the NFCRA (e.g., when $D = 9.5$ and $r_0 = 0.2$, the value of BCE of the SNACRA is approximately equal to that of the NFCRA, but the number of the elements arranged in the SNACRA is 46.8% less than that in the NFCRA. And, it can be seen that the SNACRA has fewer elements and lower CSL after comparing Figure 10 with Figure 11.); (II) the sparsity ratio γ decreases with the size of the array aperture (e.g., $\gamma\,|_{D=4.5\lambda,r_0=0.1} =$

Table 2. Comparison of synthesis numerical results between the SNACRA and the NFCRA.

$D(\lambda)$	r_0	SNACRA				NFCRA				γ (%)
		M	N	BCE (%)	CSL (dB)	M	N	BCE (%)	CSL (dB)	
4.5	0.1	4	46	76.65	−3.21	5	71	76.06	−3.14	64.79
	0.2		48	97.87	−12.08			97.69	−11.94	67.61
	0.4		48	99.99	−41.23			99.99	−37.66	67.61
9.5	0.05	7	156	77.45	−3.35	10	295	77.10	−3.31	52.88
	0.1		153	97.96	−12.15			97.94	−11.97	51.86
	0.2		157	99.99	−42.05			99.99	−36.60	53.22
19.5	0.025	13	534	77.71	−3.76	20	1217	77.59	−3.74	43.88
	0.05		532	98.00	−12.38			97.91	−12.34	43.71
	0.05		550	99.85	−32.64			99.80	−31.85	45.19

64.79% *vs.* $\gamma|_{D=9.5\lambda,r_0=0.1} = 51.86\%$ *vs.* $\gamma|_{D=19.5\lambda,r_0=0.1} = 45.19\%$.).

The SUACRA, proposed in [15], includes two cases. In first case, the aperture diameter D, inception angle θ_0, and ring number M are set as 4.5λ, 0.201, and 5, respectively. In the second case, $D = 4.5\lambda$, $\theta_0 = 0.107$, and $M = 8$. The value of $d_{\min}$ is set as 0.4λ in both cases. For the comparison of the synthesized performance between the SNACRA and the SUACRA, the values of D, θ_0, and $d_{\min}$ are set the same as those in [15]. The synthesized results of the two kinds of arrays are listed in Table 3.

Table 3. Comparison of synthesis numerical results between the SNACRA and the SUACRA IN [15].

$D(\lambda)$	θ_0	SNACRA				SUACRA			
		M	N	BCE (%)	CSL (dB)	M	N	BCE (%)	CSL (dB)
4.5	0.201	4	48	97.84	−11.97	5	68	91.06	−9.44
9.5	0.107	7	155	98.60	−13.75	10	224	92.53	−10.74

Compared to the SUACRA, the SNACRA saves 29.4% elements and has 6.78% higher BCE and 2.53 dB lower CSL when $D = 4.5\lambda$ and $\theta_0 = 0.201$. When $D = 9.5\lambda$ and $\theta_0 = 0.107$, the SNACRA reduces elements by 30.8%, improves BCE by 6.07%, and drops CSL by 3.01 dB, compared to the SUACRA. The layout, excitation, and power pattern of SNACRAs at the two cases are given in Figure 12 and Figure 13. (For the convenience of comparison, the descriptive style of the power pattern is the

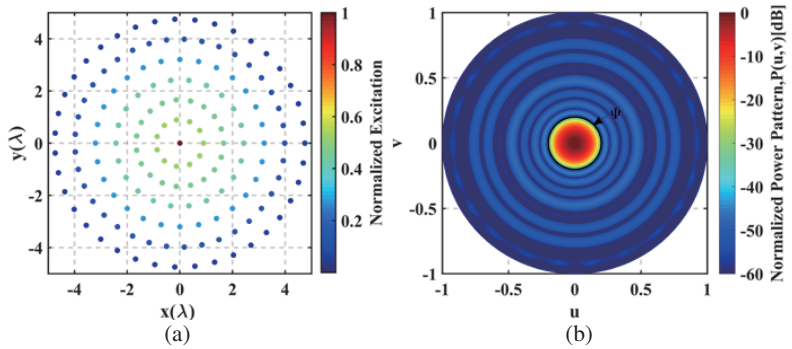

Figure 10. Synthesized results of the SNACRA ($D = 9.5\lambda$ and $r_0 = 0.2$) (a) layout and weight, (b) radiation power.

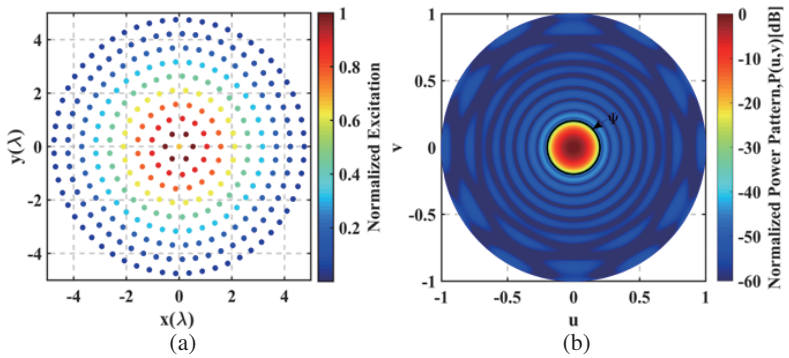

Figure 11. Synthesized results of the NFCRA ($D = 9.5\lambda$ and $r_0 = 0.2$) (a) layout and weight, (b) radiation power.

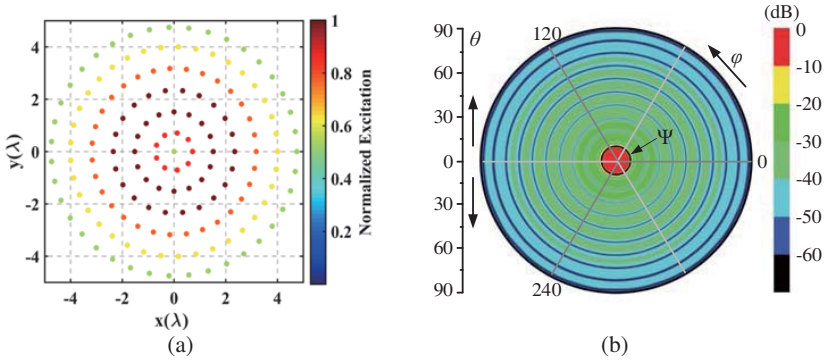

Figure 12. Synthesized results of the SNACRA ($D = 9.5\lambda$ and $\theta_0 = 0.107$) (a) layout and weight, (b) power pattern.

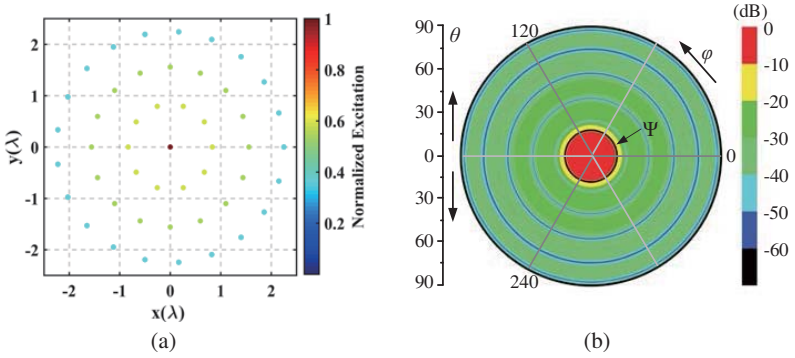

Figure 13. Synthesized results of the SNACRA ($D = 4.5\lambda$ and $\theta_0 = 0.107$) (a) layout and weight, (b) power pattern.

same as that in [15].) By comparing the power patterns between them, we can see that the SNACRA can concentrate more microwave power on the receiving area than the SUACRA, which proves that the SNACRA is more suitable for MPT.

The CSNPA, proposed in [12], is formed by removing some elements on the edge of square-lattice array to change the array aperture shape from square to circle. For further proving that the SNACRA has a good performance for MPT, multiple sets of initial parameters and synthesized results of the CSNPA and the SNACRA are given in Table 4.

Compared the performance parameters (including BCE and CSL) of the CSNPA with those of the SNACRA, the synthesized performance of the SNACRA has notable promotion, especially when

Table 4. Comparison of synthesis numerical results between the SNACRA and the CSNPA IN [12].

D (λ)	r_0	SNACRA			CSNPA		
		N	BCE (%)	CSL (dB)	N	BCE (%)	CSL (dB)
4.5	0.1	46	76.65	−3.21	76	43.61	−2.23
	0.2	48	97.87	−12.08		81.54	−6.62
	0.4	48	99.99	−41.23		99.44	−25.97
7	0.067	88	77.39	−3.35	177	44.48	−2.29
	0.133	90	97.95	−12.46		80.84	−6.54
	0.267	87	99.95	−37.25		99.35	−26.77
9.5	0.05	156	77.45	−3.35	316	77.59	−2.26
	0.1	153	97.96	−12.15		97.91	−6.21
	0.2	157	99.99	−42.05		99.80	−27.62

the receiving area is small. (e.g., when $D = 7\lambda$ and $r_0 = 0.133$, the SNACRA can save 50.9% elements and has 17.55% higher BCE and 6.01 dB lower CSL than the CSNPA). The excitation of each element within the CSNPA is a complex number and different, which greatly increases the complexity of the feed network. However, for the SNACRA, the excitation on the same ring is equal, and the excitations of all elements are real numbers rather than plurals, which can simplify the feed circuit and reduce the cost of MPT systems.

4.3. Performance of BAS Algorithm

At the end of this section, in order to prove the stability and efficiency of BAS algorithm when it is applied to the SNACRA synthesis, we compare it with GA. It should be pointed out that in the following comparative cases, only the first step of the synthesis algorithm adopts different optimization algorithms (BAS and GA), and the other steps and parameters are the same.

Firstly, when $D = 9.5\lambda$ and $r_0 = 0.1$, each algorithm is simulated three times. The number of iterations is set as 200 on each optimization. The fitness curves of six times optimization are plotted in Figure 14(a). Compared to GA, BAS algorithm is more stable, since three times optimization curves of BAS algorithm almost coincide after about 70 generations. BAS algorithm can get bigger BCE, since the fitness of BAS after stabilization is larger than that of GA.

Secondly, we repeat the above experiments under different apertures radius D and receiving areas radius r_0, then calculate the average time of three times optimization of these two algorithms. The

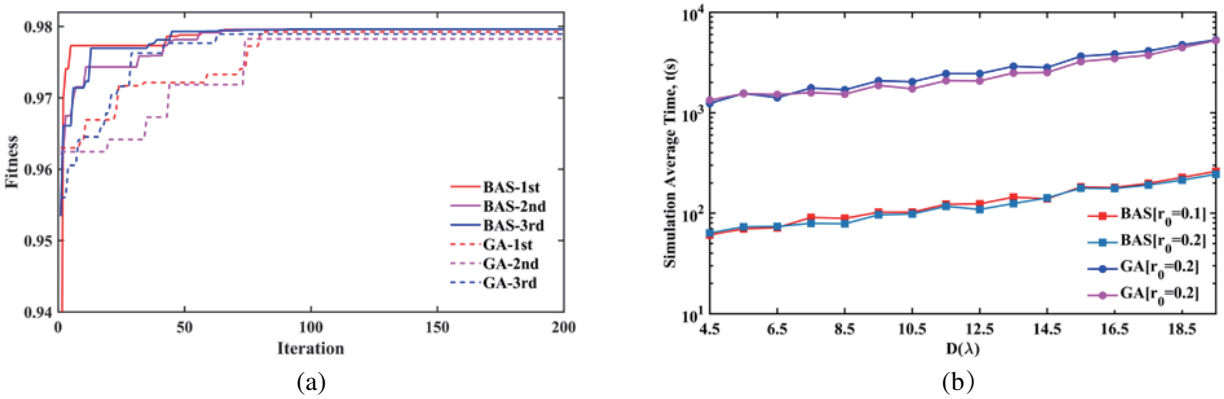

(a) (b)

Figure 14. Comparison of different optimization algorithms (BAS and GA) (a) Fitness variation curves, (b) time of optimization.

results are shown in Figure 14(b). Obviously, (I) the average optimization time increases with the size of the aperture for both algorithms; (II) under the same aperture, the receiving area size has little effect on the average optimization time; (III) the average optimization time of BAS algorithm is far less than that of GA, which indicate that BAS algorithm has higher efficient dealing with the problems of the SNACRA synthesis.

5. CONCLUSION

In this paper, we propose a sparse array model of the concentric ring array with nonuniform ring amplitude, which is SNACRA, for microwave power transmission. After deriving the maximum *BCE* of the SNACRA, we propose a novel two-step synthesis method for the SNACRA to maximize the *BCE*. Under the limitation of the minimum array element spacing, the first step is to maximize the *BCE* of the SNACRA by optimizing the ring radius, and the second step is to discretize the equivalent continuous amplitude by optimizing the number of array elements on each ring. Through the above two-step synthesis method, we can quickly and accurately obtain the optimal synthesis parameters of the SNACRA, including maximum *BCE*, array element position, number of array elements, element amplitude, *CSL*, and power pattern.

Besides, we conduct a large number of synthesis experiments to prove the advantage of the proposed array model and the validity of the synthesis method. Firstly, we discuss effects of some parameters, including the number of rings, the size of array aperture and receiving area, on the synthesis results, which can provide some reference for practical application. Secondly, in order to prove that the SNACRA is more advantageous for microwave power transmission, we compare the results of the synthesized SNACRA with those of other three circular aperture arrays for microwave power transmission, including SUACRA in [15], NFCRA, and CSNAP in [12]. Massive simulation results show that the SNACRA can obtain higher *BCE* and lower *CSL* with fewer elements and relatively simple feed network.

In addition, the BAS algorithm is used for arrays synthesis for the first time. In order to prove its excellent performance on the SNACRA optimization, we compare it with GA in optimization time and stability. The conclusion is that the BAS algorithm can synthesize the SNACRA quickly and stably compared to GA, which can be applied to large-scale array synthesis for long-distance MPT.

ACKNOWLEDGMENT

This work was supported by the National Natural Science Foundation of China (Grant No. 51877151) and the Program for Innovative Research Team in University of Tianjin (Grant No. TD13-5040).

REFERENCES

1. Upasani, D. E., S. B. Shrote, and V. P. Wani, "Wireless electrical power transmission," *Int. J. Comput. Appl.*, Vol. 1, No. 18, 6–10, 2010.
2. Li, X., J. Zhou, B. Y. Duan, et al., "Performance of planar arrays for microwave power transmission with position errors," *IEEE Antennas Wireless Propag. Lett.*, Vol. 14, 1794–1797, 2015.
3. Hui, Q., K. Jin, and X. Zhu, "Directional radiation technique for maximum receiving power in microwave power transmission system," *IEEE Transactions on Industrial Electronics*, Vol. 67, No. 8, 6376–6386, 2020.
4. Xia, M. and S. Aissa, "On the efficiency of far-field wireless power transfer," *IEEE Transactions on Signal Processing*, Vol. 63, No. 11, 2835–2847, 2015.
5. Shinohara, N., "Power without wires," *IEEE Microw. Mag.*, Vol. 12, No. 7, 64–73, 2011.
6. Gavan, J. and S. Tapuch, "Microwave wireless-power transmission to high-altitude-platform systems," *Radio Sci. Bull.*, Vol. 83, No. 3, 25–42, 2017.
7. Sasaki, S., K. Tanaka, and K. I. Maki, "Microwave power transmission technologies for solar power satellites," *Proc. IEEE*, Vol. 101, No. 6, 1438–1447, 2013.

8. Li, X., K. M. Luk, and B. Duan, "Multiobjective optimal antenna synthesis for microwave wireless power transmission," *IEEE Transactions on Antennas and Propagation*, Vol. 67, No. 4, 2739–2744, 2019.
9. Safar, M. A. and A. S. Al-Zayed, "A novel three-dimensional beamforming antenna array for wireless power focusing," *Mathematical Problems in Engineering*, 1–8, 2016.
10. Oliveri, G., P. Rocca, F. Viani, F. Robol, and A. Massa, "Latest advances and innovative solutions in antenna array synthesis for microwave wireless power transmission," *2012 IEEE MTT-S International Microwave Workshop Series on Innovative Wireless Power Transmission: Technologies, Systems, and Applications*, 71–73, Kyoto, 2012.
11. Massa, A., G. Oliveri, F. Wani, et al., "Array designs for long-distance wireless power transmission: State-of-the-art and innovative solutions," *Proc. IEEE*, Vol. 101, No. 6, 146–1481, 2013.
12. Oliveri, G., L. Poli, and A. Massa, "Maximum efficiency beam synthesis of radiating planar arrays for wireless power transmission," *IEEE Transactions on Antennas and Propagation*, Vol. 61, No. 5, 2490–2499, 2013.
13. Takahashi, T., T. Mizuno, M. Sawa, et al., "Development of phased array for high accurate microwave power transmission," *Proc. IEEE Int. Microw. Workshop Ser. Innovative Wireless Power Transm., Technol. Syst. Appl.*, 157–160, Kyoto, Japan, May 2011.
14. Li, X., B. Duan, L. Zhou, et al., "Planar array synthesis for optimal microwave power transmission with multiple constraints," *IEEE Antennas Wireless Propag. Lett.*, Vol. 16, No. 5, 70–73, 2017.
15. Zhou, H. W., X. X. Yang, and S. Rahim, "Synthesis of the sparse uniform-amplitude concentric ring transmitting array for optimal microwave power transmission," *Int. J. Antennas and Propagation*, Vol. 2018, 1–8, 2018.
16. Rocca, P., G. Oliveri, and A. Massa, "Innovative array designs for wireless power transmission," *Proc. IEEE Int. Microw. Workshop Ser. Innovative Wireless Power Transm., Technol. Syst. Appl.*, 279–282, Kyoto, Japan, May 2011.
17. Xiangyuan, J. and L. Shuai, "BAS: Beetle antennae search algorithm for optimization problems," *International Journal of Robotics and Control*, Vol. 1, No. 1, 1–5, 2018.
18. Balanis, C. A., *Antenna Theory: Analysis and Design*, 3rd Edition, Chapter 6, John Wiley & Sons, 2005.
19. Guo, Q., C. Chen, and Y. Jiang, "An effective approach for the synthesis of uniform amplitude concentric ring arrays," *IEEE Antennas Wireless Propag. Lett.*, Vol. 16, 2558–2561, 2017.
20. Zheng, Z., Y. Yan, L. Zhang, et al., "Research on genetic algorithm of antenna arrays beam shaping with side lobe suppression," *Journal of Electronics and Information Technology*, Vol. 39, No. 3, 690–696, 2017.